4170 *Biochemistry* **2009,** *48,* 4170–4180
DOI:10.1021/bi802331r

BIOCHEMISTRY
including biophysical chemistry & molecular biology
Article

Kinetic Mechanism of Pyranose 2-Oxidase from *Trametes multicolor*†

Methinee Prongjit,‡ Jeerus Sucharitakul,§ Thanyaporn Wongnate,‡ Dietmar Haltrich,∥ and Pimchai Chaiyen*,‡

‡*Department of Biochemistry and Center for Excellence in Protein Structure and Function, Faculty of Science, Mahidol University, Bangkok 10400, Thailand,* §*Department of Biochemistry, Faculty of Dentistry, Chulalongkorn University, Henri-Dunant Road, Patumwan, Bangkok 10300, Thailand, and* ∥*Department of Food Science and Technology, BOKU-University of Natural Sources and Applied Life Sciences, A-1190 Vienna, Austria*

Received December 21, 2008. Revised Manuscript Received March 24, 2009

ABSTRACT: Pyranose 2-oxidase (P2O) from *Trametes multicolor* is a flavoprotein oxidase that catalyzes the oxidation of aldopyranoses by molecular oxygen to yield the corresponding 2-keto-aldoses and hydrogen peroxide. P2O is the first enzyme in the class of flavoprotein oxidases, for which a C4a-hydroperoxy-flavin adenine dinucleotide (FAD) intermediate has been detected during the oxidative half-reaction. In this study, the reduction kinetics of P2O by D-glucose and 2-*d*-D-glucose at pH 7.0 was investigated using stopped-flow techniques. The results indicate that D-glucose binds to the enzyme with a two-step binding process; the first step is the initial complex formation, while the second step is the isomerization to form an active Michaelis complex (E-Fl_{ox}:G). Interestingly, the complex (E-Fl_{ox}:G) showed greater absorbance at 395 nm than the oxidized enzyme, and the isomerization process showed a significant inverse isotope effect, implying that the C2−H bond of D-glucose is more rigid in the E-Fl_{ox}:G complex than in the free form. A large normal primary isotope effect (k_H/k_D = 8.84) was detected in the flavin reduction step. Steady-state kinetics at pH 7.0 shows a series of parallel lines. Kinetics of formation and decay of C-4a-hydroperoxy-FAD is the same in absence and presence of 2-keto-D-glucose, implying that the sugar does not bind to P2O during the oxidative half-reaction. This suggests that the kinetic mechanism of P2O is likely to be the ping-pong-type where the sugar product leaves prior to the oxygen reaction. The movement of the active site loop when oxygen is present is proposed to facilitate the release of the sugar product. Correlation between data from pre-steady-state and steady-state kinetics has shown that the overall turnover of the reaction is limited by the steps of flavin reduction and decay of C4a-hydroperoxy-FAD.

Pyranose 2-oxidase (P2O;[1] pyranose:oxygen 2-oxidoreductase; EC 1.13.10) is a flavoprotein oxidase catalyzing the oxidation of several aldopyranoses by molecular oxygen at the C2 position to yield the corresponding 2-keto-aldoses and hydrogen peroxide (Scheme 1) (*1*). The enzyme was identified and isolated from several species of fungi (*2*) and is thought to be involved in lignin degradation by providing H_2O_2 for lignin peroxidase (*3*). H_2O_2 production by P2O can also be important for maintaining an oxidative stress level that helps control the growth of other competing organisms (*4*). The regiospecific oxidation at the pyranose C2 position catalyzed by P2O is a very useful reaction for carbohydrate syntheses since it can be applied in the syntheses of D-tagatose (*5*), cortalcerone (*6*), and other valuable sugar synthons (*2*, *4*).

P2O from *Trametes multicolor* is a homotetrameric enzyme with a native molecular mass of 270 kDa (subunit molecular mass of 68 kDa) (*1*). Each subunit contains one flavin adenine dinucleotide (FAD) covalently attached to the N3 of His167 (*7*). The enzyme sequence and structure indicate that P2O belongs to the glucose−methanol−choline (GMC) oxidoreductase enzyme superfamily of flavoproteins (*8*, *9*). The three-dimensional structures of P2O show the involvement of a dynamic loop located at the active site of the enzyme in substrate binding. The loop

†This work was supported by The Thailand Research Fund through Grant Nos. BRG5180002 (to P.C.), MRG4980117 (to J.S.), and PHD/0151/2547 of the Royal Golden Jubilee Ph.D. program (to M.P.). Grants from the Faculty of Science, Mahidol University (to P.C.), from the Faculty of Dentistry Chulalongkorn University (to J.S.), and from National Science and Technology Development Agency (to T.W.) are also acknowledged. D.H. was supported by a grant from the Austrian Research Foundation (FWF Translational Project L213-B11).

*To whom correspondence should be addressed. Mailing address: Pimchai Chaiyen, Department of Biochemistry and Center for Excellence in Protein Structure and Function, Faculty of Science, Mahidol University, Rama 6 Road, Bangkok, 10400, Thailand. Tel: 662-2015596. Fax: 662-3547174. E-mail: scpcy@mahidol.ac.th.

[1]Abbreviations: P2O, pyranose oxidase; FAD, flavin adenine dinucleotide; k_{obs}, observed rate constant; 2FG, 2-fluoro-deoxy-D-glucose; GMC, glucose−methanol−choline family; ABTS, 2,2-azino-bis(3-ethylbenzthiazoline-6-sulfonic acid diammonium salt); E-Fl_{ox}, P2O in the oxidized form; E-Fl_{red}, P2O in the reduced form; E-Fl_{ox}/G, a complex of P2O and D-glucose; E-Fl-OOH, a C4a-hydroperoxy-FAD intermediate.

 Published on Web 3/24/2009

Scheme 1: Reaction of Pyranose 2-Oxidase

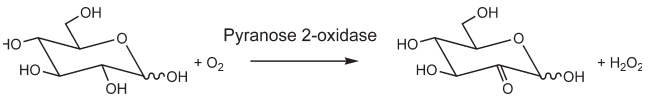

swings out (open conformation) when the substrate analogue (2-fluoro-2-deoxy-D-glucose, 2FG) (*10*) or the 2-keto-D-glucose product is bound (*11*) and closes in (closed conformation) to shield the active site from the bulk solvent upon the binding of a small molecule such as acetate (*9*). The reaction catalyzed by P2O can be divided into a reductive half-reaction where the FAD cofactor is reduced by a sugar substrate and an oxidative half-reaction where the reduced FAD is oxidized by molecular oxygen or other electron acceptors such as benzoquinones or metal ions (*1*). It has been proposed that the enzyme assumes the open conformation during the reductive half-reaction and the closed conformation during the oxidative half-reaction (*10*). Recent investigation on steady-state kinetics of P2O from *T. ochracea* shows the difference in the kinetic mechanism at pH below and above 7.0 (*12*). Investigation on the oxidative half-reaction of P2O has shown for the first time the presence of a C4a-hydroperoxy-flavin intermediate in the class of flavoprotein oxidases (*13*). Similarly, the C4a-adduct intermediate was detected in the crystal structure of choline oxidase (*14*). These two reports suggest that the C4a-hydroperoxy-flavin, although it has long been thought to be common only in flavoprotein oxygenases (*15*, *16*), may also be common for flavoprotein oxidases. The finding also implies that the active sites of oxidases and oxygenases, although different, are both capable of accommodating the formation of the C4a-hydroperoxy-flavin. Therefore, a thorough understanding of the reaction mechanism of P2O is necessary for serving as a foundation for future in-depth investigations on the structure and mechanism of P2O.

In this study, the reduction kinetics of P2O by D-glucose was investigated using stopped-flow techniques to measure rate constants associated with each step in the reaction. The reduction by 2-*d*-D-glucose showed a large normal primary isotope effect at the step involved with the hydride transfer. Interestingly, an intermediate with an absorption coefficient at 395 nm greater than that of the oxidized enzyme was detected upon the binding of D-glucose, and this binding showed a significant inverse isotope effect. Comparison between pre-steady-state and steady-state kinetics has identified the steps that limit the overall turnover of the reaction.

MATERIALS AND METHODS

Reagents. D-Glucose (99.5% purity), 2-*d*-D-glucose, and horseradish peroxidase were purchased from Sigma-Aldrich. ABTS [2,2′-azino-bis(3 -ethylbenzenethiazoline-6-sulfonic acid) diammonium salt] was purchased from Roche (Germany). Concentrations of the following compounds were determined using the known absorption coefficients at pH 7.0: $\varepsilon_{403} = 100 \times 10^3\ M^{-1}\ cm^{-1}$ for horseradish peroxidase; $\varepsilon_{458} = 11.3 \times 10^3\ M^{-1}\ cm^{-1}$ for the value of FAD covalently linked to each subunit of P2O (*13*).

Spectroscopic Studies. UV−visible absorbance spectra were recorded with a Hewlett-Packard diode array spectrophotometer (HP8453), a Shimadzu 2501PC spectrophotometer or a Cary 300Bio double-beam spectrophotometer. All spectral instruments were equipped with thermostatted cell compartments. Enzyme activity was determined by a continuous assay based on a coupled reaction of horseradish peroxidase and its substrate ABTS as previously described (*17*). Initial rates were monitored from the increase of absorbance at 420 nm resulting from the oxidation of ABTS by H_2O_2 using the molar absorption coefficient of $4.2 \times 10^5\ M^{-1}\ cm^{-1}$ (per one mole of D-glucose consumed). Steady-state kinetics data were analyzed using the Enzfitter program (BIOSOFT, Cambridge, UK) for a bisubstrate reaction.

Rapid Reaction Experiments. Reactions were carried out in 50 mM sodium phosphate, pH 7.0, 4 °C, unless otherwise specified. Rapid kinetics measurements were performed with a Hi-Tech Scientific model SF-61DX stopped-flow spectrophotometer in single-mixing or double-mixing mode. The optical path length of the observation cell was 1 cm. The stopped-flow apparatus was made anaerobic by flushing the flow system with an anaerobic buffer solution containing 400 μM protocatechuic acid (PCA) and ~1 μg/mL protocatechuic acid dioxygenase (PCD). The buffer was made anaerobic by equilibrating with oxygen-free nitrogen (ultrahigh pure grade) that had been passed through an Oxyclear oxygen removal column (Labclear) using an anaerobic glovebox or an anaerobic train (*18*). The PCA/PCD solution was allowed to stand in the flow system overnight. The flow unit was then rinsed with the anaerobic buffer before experiments. For studying the reduction of the enzyme by D-glucose and 2-*d*-D-glucose, the oxidized enzyme solution was made anaerobic and placed in a tonometer before being loaded onto the stopped-flow machine. The substrate solutions (~3 mL) at various concentrations were placed in 5 mL glass syringes, made anaerobic by bubbling with oxygen-free nitrogen for 8 min, and loaded onto the stopped-flow machine. The oxidized enzyme and substrate solutions were mixed under the stopped-flow spectrophotometer and monitored at various wavelengths in the region of 350−530 nm. For studying reactions of the reduced enzyme with oxygen, an anaerobic solution of the oxidized enzyme was placed in a glass tonometer and stoichiometrically reduced with a solution of sugar substrate (~10 mM in 50 mM sodium phosphate, pH 7.0) or dithionite solution (5 mg/mL in 100 mM potassium phosphate, pH 7.0) delivered from a syringe attached to the tonometer. The reduced enzyme solution was mixed with buffers containing various oxygen concentrations, which were prepared by equilibrating the buffer with air, 50% of a certified oxygen-in-nitrogen gas mixture, 100% oxygen, or 100% oxygen on ice in order to achieve 200% oxygen saturation. Kinetics of the reactions were followed by monitoring the flavin absorbance at various wavelengths between 350 and 530 nm. Apparent rate constants (k_{obs}) from kinetic traces were calculated from exponential fits using the softwares Kinetic

Studio (Hi-Tech Scientific, Salisbury, UK) or Program A (written at the University of Michigan by Rong Chang, Jung-yen Chiu, Joel Dinverno, and D. P. Ballou). Rate constants were determined from plots of k_{obs} versus sugar or oxygen concentrations using a Marquardt−Levenberg nonlinear fit algorithm that is included in KaleidaGraph (Synergy Software). Simulations were performed by numerical methods using the fourth-order Runge−Kutta algorithm implemented in Berkeley Madonna 8.3 with time step of 10^{-3} s. A model of four-step reversible reaction was used.

Analysis of Kinetic Parameters of a Three-Step Reaction. Expression of experimental observed rate constants (reciprocal of relaxation time ($1/\tau$)) in terms of specific rate constants was derived according to the method described by Hammes and Schimmel (*19*, *20*); *n* relaxation times according to the kinetic model in Scheme A1 are the *n* eigenvalues of the secular eq A1.

Scheme A1

$$E_{ox} \underset{k_{-1}}{\overset{k_1[G]}{\rightleftharpoons}} E_{ox} : G* \underset{k_{-2}}{\overset{k_2}{\rightleftharpoons}} E_{ox} : G \underset{k_{-3}}{\overset{k_3}{\rightleftharpoons}} E_{red} : P$$

$$\left| b - \frac{1}{\tau} I \right| = 0 \qquad \text{(A1)}$$

where $|b - (1/\tau)I|$ is the determinant of the matrix $|b - (1/\tau)I|$, I is the unit matrix (identity matrix), and $\mathbf{b}$ is a matrix with all elements equal to zero except

$$b_{ii} = k_i + k_{-i}$$

$$b_{ij} = -k_i; \quad j = i-1, \quad i \neq 1$$

$$b_{ij} = -k_{-i}; \quad j = i+1, \quad i \neq n$$

Therefore, for a three-step reaction as in Scheme A1, the matrix $\mathbf{b}$ is

$$\mathbf{b} = \begin{bmatrix} k_1' + k_{-1} & -k_{-1} & 0 \\ -k_2 & k_2 + k_{-2} & -k_{-2} \\ 0 & -k_3 & k_3 + k_{-3} \end{bmatrix}; \quad k_1' = k_1[G]$$

Reciprocal of relaxation times can be calculated by the determinantal method. If the *j*th reaction is assumed to be slowly equilibrated relative to all other reactions, then the relaxation time for this step is

$$\frac{1}{\tau_j} = \frac{|\mathbf{b}|}{|\mathbf{b}_{jj}|}$$

$\mathbf{b}_{jj}$ is the matrix obtained by deleting the *j*th row and *j*th column of $\mathbf{b}$.

$$\mathbf{b}_{33} = \begin{bmatrix} k_1' + k_{-1} & -k_{-1} \\ -k_2 & k_2 + k_{-2} \end{bmatrix}$$

$$\text{when} \quad j = 3, \quad \frac{1}{\tau_3} = \frac{|\mathbf{b}|}{|b_{33}|} = k_{obs}iii \qquad \text{(A2)}$$

Analysis of the data in Figure 1 indicated that the rate of the flavin reduction is about 10-times slower than the rates of the two preceding steps. This indicates that the assumption above is valid for our case and eq A2 can be used for calculating $k_{obs}iii$.

$$\begin{aligned} |\mathbf{b}| &= k_1'k_{-2}k_{-3} + k_1'k_2k_{-3} + k_1'k_{-2}k_3 + k_1'k_2k_3 \\ &\quad + k_{-1}k_{-2}k_{-3} + k_{-1}k_2k_{-3} + k_{-1}k_{-2}k_3 \\ &\quad + k_{-1}k_2k_3 - k_1'k_{-2}k_3 - k_{-1}k_{-2}k_3 - k_{-1}k_2k_3 \\ &\quad - k_{-1}k_2k_{-3} = k_1'k_2k_3 + k_1'k_2k_{-3} + k_1'k_{-2}k_{-3} \\ &\quad + k_{-1}k_{-2}k_{-3} \end{aligned}$$

$$\begin{aligned} |\mathbf{b}_{33}| &= k_1'k_2 + k_1'k_{-2} + k_{-1}k_2 + k_{-1}k_{-2} - k_{-1}k_2 \\ &= k_1'k_2 + k_1'k_{-2} + k_{-1}k_{-2} \end{aligned}$$

$$\begin{aligned} k_{obs}iii &= \frac{|\mathbf{b}|}{|\mathbf{b}_{33}|} \\ &= \frac{k_1'k_2k_3 + k_1'k_2k_{-3} + k_1'k_{-2}k_{-3} + k_{-1}k_{-2}k_{-3}}{k_1'k_2 + k_1'k_{-2} + k_{-1}k_{-2}} \\ &= \frac{k_1'k_2k_3 + k_{-3}(k_1'k_2 + k_1'k_{-2} + k_{-1}k_{-2})}{k_1'k_2 + k_1'k_{-2} + k_{-1}k_{-2}} \\ &= \frac{k_1'k_2k_3}{k_1'(k_2 + k_{-2}) + k_{-1}k_{-2}} + k_{-3} \\ &= \frac{\frac{k_2k_3}{(k_2 + k_{-2})}[G]}{K_d\left(\frac{k_{-2}}{k_2 + k_{-2}}\right) + [G]} + k_{-3} \end{aligned}$$

Likewise, k_{obs} of the previous step can be calculated from

$$\frac{1}{\tau_2} = \frac{|\mathbf{b}_{33}|}{|\mathbf{b}_{33_{22}}|} = k_{obs}ii$$

$$k_{obs}ii = \frac{k_2[G]}{K_d + [G]} + k_{-2}$$

RESULTS

Reduction of P2O by D*-Glucose*. A solution of the oxidized enzyme in 50 mM sodium phosphate, pH 7.0, was mixed with solutions of the same buffer containing various concentrations of D-glucose using the stopped-flow spectrophotometer under anaerobic conditions (Figure 1). The flavin reduction was monitored in 10 nm intervals within the range of 350−530 nm. The data at 395 and 458 nm, where maximum changes in absorbance were attained, were used for kinetic analysis. Kinetic traces at 395 nm showed three exponential phases (Figure 1A). At the highest concentration of D-glucose (50 mM), the data showed an absorbance increase during the first phase (0.002−0.02 s), while the second phase (0.02−0.5 s) was characterized by a decrease in absorbance. Only the kinetics of the second phase coincided with the kinetics of a large amplitude decrease at 458 nm, whereas the first phase detected at 395 nm occurred without any correlation to the flavin reduction monitored at 458 nm (Figure 1A,B). The third phase showed very slow kinetics with a small amplitude change at 395 nm and no change at 458 nm. The change of this phase completed at ~2000 s and corresponded to a rate constant of 0.002 s^{-1} (inset in Figure 1A).

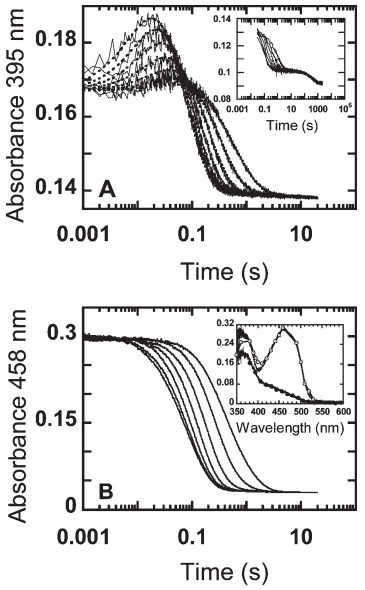

FIGURE 1: Kinetic traces of the reduction of P2O by D-glucose. A solution of the enzyme (28 μM) was mixed with solutions of D-glucose at concentrations of 0.8, 1.6, 3.2, 6.4, 12.8, 25, and 50 mM in 50 mM sodium phosphate (pH 7.0). All concentrations are as after mixing. The reactions were performed using the stopped-flow spectrophotometer at 4 °C under anaerobic conditions. Data were fitted with three exponentials and show that kinetics of both wavelengths (395 and 458 nm) are similar. (A) The reactions monitored at 395 nm show a large absorbance increase for the first exponential phase. The lower to upper traces are from lower to higher concentrations of D-glucose. Dotted lines represent simulations using the model in Scheme 2 and the following parameters: $k_1 = 5.8 \times 10^4\ s^{-1}$; $k_{-1} = 2.5 \times 10^3\ s^{-1}$; $k_2 = 160\ s^{-1}$; $k_{-2} = 10\ s^{-1}$; $k_3 = 15\ s^{-1}$; $k_{-3} = 0\ s^{-1}$; $k_4 = 0.0015\ s^{-1}$; $k_{-4} = 0\ s^{-1}$; ε_{395}(E-Fl$_{ox}$) = 6300 $M^{-1}\ cm^{-1}$; ε_{395}(E-Fl$_{ox}$:G*) = 6300 $M^{-1}\ cm^{-1}$; ε_{395}(E-Fl$_{ox}$:G) = 7600 $M^{-1}\ cm^{-1}$; ε_{395}(E-Fl$_{red}$:P) = 5300 $M^{-1}\ cm^{-1}$; and ε_{395}(E-Fl$_{red}$) = 4100 $M^{-1}\ cm^{-1}$. In the inset, the third phase showing a decrease in absorbance at 395 nm was very slow and independent of substrate concentration. (B) Kinetic traces from the absorbance change at 458 nm. Traces from the right to the left are from lower to higher concentrations of D-glucose. Inset shows spectra of the flavin species including the oxidized enzyme (solid line), the intermediate formed after the first observed phase using 25 mM D-glucose (E-Fl$_{ox}$:G, open-circle line), and the reduced enzyme (filled-circle line).

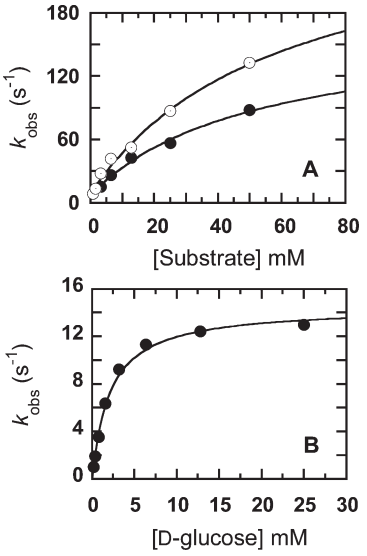

FIGURE 2: Kinetics of the reductive half-reaction of P2O at various D-glucose and 2-*d*-D-glucose concentrations. The observed rate constants (k_{obs}) were obtained from kinetic analysis of the traces from Figures 1 and 3. (A) The filled-circle line (●) shows a plot of k_{obs} obtained from the first phase of the reduction (large absorbance change at 395 nm) versus D-glucose concentrations. The open-circle line (○) shows a plot of k_{obs} obtained from the first phase of the reduction versus concentrations of the deuterated substrate (2-*d*-D-glucose). (B) A plot of k_{obs} obtained from the second phase of the reduction (large absorbance change at 458 nm) versus D-glucose concentrations.

The k_{obs} values of the first and second phases were separated by the ratio of $k_{obs1}/k_{obs2} \approx 10$ throughout all D-glucose concentrations, which is well above the limit value (the ratio of $k_{obs1}/k_{obs2} = 3$) that does not allow two consecutive exponentials to be unambiguously identified (*21*). Therefore, k_{obs} of both phases in Figure 1 can be accurately estimated; k_{obs}, however, cannot be simply equated with a specific rate constant of any particular step as illustrated in refs (*13*, *22*). Since observed rate constants (k_{obs}) of the first phase (data from A_{395}) are hyperbolically dependent on D-glucose concentrations (Figure 2A), this indicates that the first observed phase is not a direct binding of D-glucose to the enzyme but it is an isomerization of an initial enzyme−substrate complex after the initial binding (*21*). The second observed phase must be the flavin reduction as indicated by a large change in absorbance at 458 and a large primary isotope effect when 2-*d*-D-glucose was used (see below). Therefore, a minimal kinetic scheme required for explaining behavior of the first and second observed phases is a three-step reaction as shown in Scheme 2. Using the method described in refs (*19* and *20*), one can derive relationships of k_{obs} and individual rate constants (Materials and Methods) and are related to our data as shown in eqs 1 and 2.

$$k_{obs}(\text{firstphase}) = \frac{k_2[G]}{K_d + [G]} + k_{-2} \quad (1)$$

$$k_{obs}(\text{secondphase}) = \frac{\frac{k_2 k_3}{(k_2 + k_{-2})}[G]}{K_d\left(\frac{k_{-2}}{k_2 + k_{-2}}\right) + [G]} + k_{-3} \quad (2)$$

A plot of k_{obs} of the first phase versus D-glucose concentrations yielded the limiting value of $\sim 162 \pm 40\ s^{-1}$ and an intercept of $8 \pm 5\ s^{-1}$ (filled-circle line in Figure 2A). This observed phase is interpreted as a rapid binding of D-glucose to form an initial enzyme−substrate complex (E-Fl$_{ox}$/G*) that is further isomerized with a forward rate constant of $\sim 162 \pm 40\ s^{-1}$ and a reverse rate constant of $8 \pm 5\ s^{-1}$ (eq 1) to form an active complex (E-Fl$_{ox}$/G) prior to the next reduction step (Scheme 2). The dissociation constant (K_d) for the initial binding was calculated from the plot in Figure 2A and eq 1 to be 52 ± 28 mM. It should be mentioned that high error values for k_2 and K_d are due to limitation of the measurement; k_{obs} of the first phase at D-glucose concentration of 100 mM and above cannot be accurately measured since viscosity of the D-glucose solution starts to interfere with the initial part of the flow. However, the values of k_2 and K_d were further verified by analysis of the second phase and kinetic simulations (see below). Absorbance at the reaction time of 0.0207 s of wavelengths in the region of 350−530 nm when 25 mM D-glucose was used was plotted in the inset of Figure 1B to represent a spectrum of the intermediate at the end of this phase.

Scheme 2: Kinetic Mechanism of the Reductive Half-Reaction of Pyranose 2-Oxidase

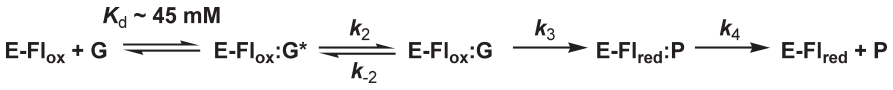

Table 1: Rate Constants According to the Kinetic Mechanism Described in Scheme 3

	from stopped-flow experiments		from simulations	
kinetic parameters	D-glucose	2-*d*-D-glucose	D-glucose	2-*d*-D-glucose
$K_d(k_{-1}/k_1)$	45 mM	~60 ± 24 mM	43 mM	43 mM
k_1			5.8×10^4 s^{-1}	5.8×10^4 s^{-1}
k_{-1}			2.5×10^3 s^{-1}	2.5×10^3 s^{-1}
k_2	~162 ± 40 s^{-1}	~269 ± 61 s^{-1}	160 s^{-1}	270 s^{-1}
k_{-2}	8 ± 5 s^{-1}	9 ± 4 s^{-1}	10 s^{-1}	3 s^{-1}
k_3	15.3 ± 0.4 s^{-1}	1.73 ± 0.05 s^{-1}	15 s^{-1}	1.7 s^{-1}
k_4	~0.002 s^{-1}	~0.002 s^{-1}	0.0015 s^{-1}	0.0015 s^{-1}
k_5	$4.3 \pm 0.4 \times 10^4$ M^{-1} s^{-1}		5.8×10^4 M^{-1} s^{-1}[a]	
k_{-5}			2 s^{-1}[a]	
k_6			18 s^{-1}[a]	

[a] Rate constants taken from the previous report (*13*).

Observed rate constants of the second phase (the flavin reduction) determined from the decrease in absorbance at both 395 and 458 nm are also hyperbolically dependent on D-glucose concentrations with the limiting value of 14.5 ± 0.4 s^{-1} and a concentration that gives half of the maximum rate of 2.1 mM (Figure 2B). According to eq 2, the limiting value is equal to $k_2k_3/(k_2 + k_{-2})$, and the D-glucose concentration giving half of the limiting value is equal to $K_d(k_{-2}/(k_2 + k_{-2}))$. Since k_2 and k_{-2} are known from the previous analysis of the first phase and eq 1, k_3 or a rate constant for the flavin reduction step was calculated to be 15.3 s^{-1} (Table 1 and Scheme 2). The K_d can be calculated from eq 2 to be 45 mM (Table1), which is in agreement with the value obtained from analysis of the first phase (52 ± 28 mM). The intercept of zero from the hyperbolic plot (Figure 2B) indicates that the reduction is essentially irreversible ($k_{-3} = 0$) in agreement with the model described in Scheme 2.

Analysis of the third phase showed that the rate is too slow (0.002 s^{-1}) to be relevant to the overall turnover (see the steady-state kinetics results) and independent of D-glucose concentration. During this phase, the flavin cofactor is in the reduced form since there is no change in the absorbance at 458 nm. This slow phase is proposed to be the release of the oxidized sugar from the reduced enzyme active site under anaerobic conditions (k_4 in Scheme 2). The independence of the rate of this phase on D-glucose concentration agrees with the model proposed in Scheme 2, which depicts the prior step, the flavin reduction, to be irreversible. The kinetic scheme proposed in Scheme 2 was further validated in the next experiment using a deuterated substrate (2-*d*-D-glucose).

In addition, the data were analyzed using kinetic simulations as described in Materials and Methods. Simulations of the data using a model in Scheme 2 and kinetic parameters $k_1 = 5.8 \times 10^4$ s^{-1}, $k_{-1} = 2.5 \times 10^3$ s^{-1}, $k_2 = 160$ s^{-1}, $k_{-2} = 10$ s^{-1}, $k_3 = 15$ s^{-1}, $k_{-3} = 0$ s^{-1}, $k_4 = 0.0015$ s^{-1}, and $k_{-4} = 0$ s^{-1}) agree well with the experimental data (dashed versus solid lines in Figure 1A). All rate constants are summarized in Table 1.

Kinetic Isotope Effects on the Reductive Half-Reaction. The reduction of P2O by 2-*d*-D-glucose was investigated under the same conditions as in the previous D-glucose section. This experiment can unambiguously identify a step involved with the transfer of a hydride equivalent from 2-*d*-D-glucose at the C2 position to the oxidized flavin. Kinetics of the reaction was monitored at the wavelengths 395 and 458 nm. The flavin reduction monitored at 395 nm showed three phases similar to the reaction of D-glucose (Figure 3). Surprisingly, observed rate constants of the first phase when 2-*d*-D-glucose was used showed faster rate constants than those of the reaction of D-glucose at all concentrations used (open-circle versus filled-circle lines in Figure 2A). The observed rate constants were hyperbolically dependent on 2-*d*-D-glucose concentrations with the limiting value of 269 ± 61 s^{-1}, the intercept of 9 ± 4 s^{-1}, and the K_d for the initial binding of ~60 ± 24 mM (eq 1). Therefore, binding of the deuterated substrate is a two-step process similar to binding of the native substrate. Although the error values of k_2 and K_d are quite high due to limitation of the measurement as mentioned in the D-glucose experiment, k_{obs} of the first phase at all concentrations of 2-*d*-D-glucose are higher than those of D-glucose, tentatively showing an inverse kinetic isotope effect of ~0.60 (Figure 2A). Simulations using the model described in Scheme 2 and parameters in Table 1 indicated that for the reaction of 2-*d*-D-glucose, besides the primary isotope effect of the reduction step (below), k_2 with the value of 270 s^{-1} (k_{2D}) is necessary for obtaining simulations that agree well with the data (Table1). This supports that an inverse isotope effect of ~0.6 is observed for k_2. Observed rate constants of the second phase of the 2-*d*-D-glucose reaction were significantly lower than those of the D-glucose reaction and hyperbolically dependent on the sugar concentrations with the limiting value of 1.67 ± 0.05 s^{-1}

(inset in Figure 3). This flavin reduction step was calculated to be $1.73 \pm 0.005\ s^{-1}$ from eq 2. These data indicate a normal primary kinetic isotope effect of 8.84 for the step of hydride transfer from D-glucose to FAD. The slow third phase found in the reaction of D-glucose (inset of Figure 1A) was also detected in the reaction of 2-*d*-D-glucose. No kinetic isotope effect was detected for this phase since the rate is in the same range as the reaction of D-glucose, $\sim 0.002\ s^{-1}$ (data not shown), supporting the idea that the last step is a slow product releasing step from the enzyme under anaerobic conditions (Schemes 2 and 3).

Kinetics of the Oxidation of the Reduced Enzyme in Absence and Presence of 2-Keto-D-glucose. Data from the previous experiment suggest that under anaerobic conditions, the 2-keto-D-glucose product slowly dissociates from the enzyme after the FAD is reduced (Scheme 2). Although this process is too slow to be involved in the overall turnover, it raises the question whether 2-keto-D-glucose is bound to the active site during the reaction of P2O with oxygen. Therefore, the oxidative half-reaction of P2O in the absence and presence of 2-keto-D-glucose were investigated and compared for their rates of the oxygen reaction. Previously, the oxidative half-reaction of P2O where the reduced enzyme was prepared by adding a stoichiometric amount of D-glucose was reported (*13*). Under this condition, 2-keto-D-glucose is likely to be absent from the enzyme active site since the preparation process prior to the experiments is longer than the rate of 2-keto-D-glucose release (k_4 in Scheme 2). The reduced P2O reacts with oxygen to form a C4a-hydroperoxy-FAD intermediate with the rate of $5.8 \times 10^4\ M^{-1}\ s^{-1}$ (k_5), which further decays to yield the oxidized enzyme and H_2O_2 with the rate constants of $18\ s^{-1}$ (k_6) as shown in Scheme 3 and Table 1 (*13*).

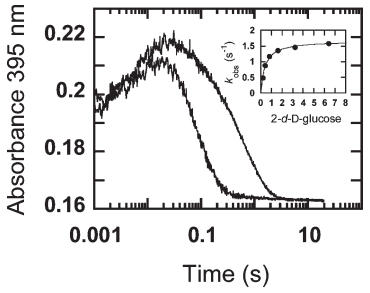

FIGURE 3: Kinetic isotope effects on the reduction of P2O. Reactions similar to those in Figure 1 were performed but using 2-*d*-D-glucose instead of D-glucose. The left trace shows the reduction of enzyme (28 μM) with 50 mM D-glucose, whereas the right trace shows the reduction of enzyme (28 μM) with 50 mM of 2-*d*-D-glucose. Both traces are monitored at 395 nm. The kinetic data show that the isotope substrate significantly lowers the rate of the second phase, indicating that this step involves a C2−H bond cleavage or a hydride transfer from D-glucose to FAD. The inset shows that the k_{obs} are hyperbolically dependent on 2-*d*-D-glucose concentrations. Rate constants from the analysis are shown in Table 1 and Scheme 3.

In order to explore the oxidative half-reaction of P2O under conditions when 2-keto-D-glucose is strictly absent, the reduced enzyme (20 μM) was prepared in this study by using a dithionite solution as a reducing agent as described in Materials and Methods. Oxidation of the free reduced enzyme was monitored using the stopped-flow spectrophotometer (Figure 4) under the same conditions as when D-glucose was used as a reducing reagent (*13*). The reaction was monitored at 395 nm for measuring the rates of the intermediate formation and decay whereas the FAD oxidation was monitored at 458 nm. The reaction showed two exponential phases (Figure 4). Observed rate constants of the first phase are linearly dependent on oxygen concentrations (The upper inset in Figure 4). A slope of the plot indicates an apparent bimolecular rate constant of $(4.8 \pm 0.2) \times 10^4\ M^{-1}\ s^{-1}$ with an intercept value of $19\ s^{-1}$ (Table 2). These values are in the same range as when D-glucose is used as a reductant, $(4.3 \pm 0.4) \times 10^4\ M^{-1}\ s^{-1}$ and $18\ s^{-1}$ for the apparent bimolecular rate constant and the intercept value, respectively (Figure 4, Table 2). Observed rate constants of the second phase are hyperbolically dependent on oxygen concentrations, approaching a value of $22 \pm 2\ s^{-1}$ (The lower inset in Figure 4), which is not different from the reaction of the enzyme reduced by D-glucose, $21 \pm 2\ s^{-1}$ (Table 2).

Kinetics of the oxidation of the reduced enzyme in the presence of 2-keto-D-glucose was furthermore explored using double-mixing stopped-flow spectrophotometry (Figure 4). The first mix was performed under anaerobic conditions by mixing the oxidized enzyme with an equivalent concentration of D-glucose. The enzyme was allowed to be fully reduced by using an age time of 350 s. Then, on the second mix, the solution from the first mix was allowed to react with buffers containing various oxygen

Scheme 3: Kinetic Mechanism of the Reaction of Pyranose 2-Oxidase

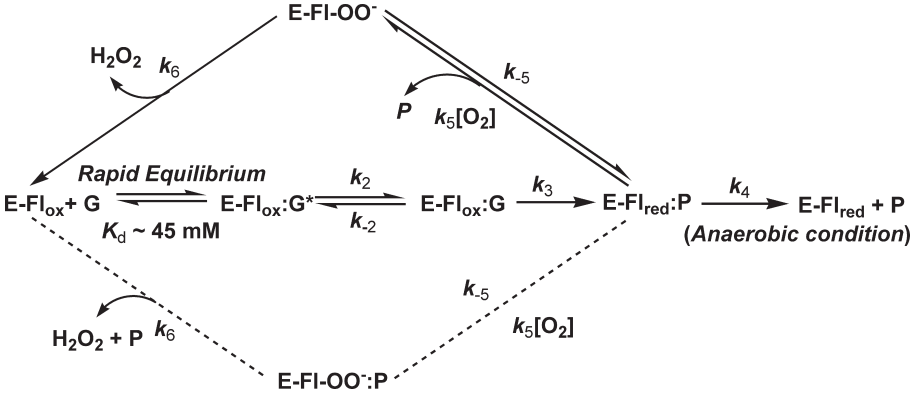

concentrations. In this experiment, the second mix was designed to take place before product release under anaerobic conditions completed (k_4, Schemes 2 and 3). The reactions were monitored at 395 and 458 nm. The traces at 395 nm from the double-mixing experiment show similar kinetics for formation and decay of C4a-hydroperoxy-FAD compared with those without 2-keto-D-glucose (dotted versus solid lines of Figure 4; Table 2). A plot of observed rate constants from the first phase versus oxygen concentration was linear (The upper inset in Figure 4), yielding the apparent bimolecular rate constant of $(4.3 \pm 0.2) \times 10^4$ M^{-1} s^{-1} and the intercept of 18 s^{-1}. Observed rate constants of the second phases were also hyperbolically dependent on oxygen concentrations with the saturation rate constant of 24 ± 2 s^{-1}. All of these values are similar to those of the reactions when 2-keto-D-glucose is strictly absent.

The results given in Figure 4 and Table 2 indicate that the reduced P2O, regardless of the method used for enzyme reduction, reacts with oxygen in the same fashion, suggesting two possible explanations. First, the presence of oxygen induces the immediate release of 2-keto-D-glucose to form the free reduced enzyme prior to formation of the C4a-hydroperoxy-FAD intermediate (upper pathway of Scheme 3). It can be envisaged that the substrate loop movement in the structure of P2O can, in principle, facilitate this release of 2-keto-D-glucose (*10*), see more in the Discussion). Another explanation for this result is that the oxidation occurs when 2-keto-D-glucose is still bound (lower pathway of Scheme 3) but the presence of 2-keto-D-glucose in the active site does not affect the oxygen reaction. Based on current data, the lower pathway of Scheme 3 is unlikely, and the upper pathway is preferred (see more in the Discussion).

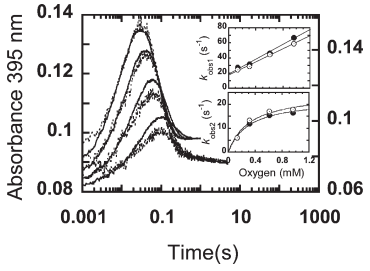

FIGURE 4: Oxidative half-reaction of P2O in the presence and absence of the 2-keto-D-glucose product. The dotted line shows kinetics of the oxidation of reduced P2O in presence of the sugar product (2-keto-D-glucose) using double-mixing stopped-flow spectrophotometry (*Y*-scale on the left axis). All reactions were performed in 50 mM sodium phosphate (pH 7.0) at 4 °C, and the absorbance change at 395 nm was monitored to detect the formation and decay of C4a-hydroperoxy-flavin. The first mix combined the oxidized enzyme (15.4 μM after mixing) with a stoichiometric amount of D-glucose (~16 μM after mixing) under anaerobic conditions using an age time of 350 s to allow the enzyme to be fully reduced. The second mix combined a solution of the reduced enzyme with the same buffer containing 0.13, 0.31, 0.61, and 0.96 mM oxygen (concentration as after mixing). The solid lines show the oxidation of the reduced enzyme (20 μM after mixing) prepared by dithionite reduction, which represents the condition when 2-keto-D-glucose is strictly absent (*Y*-scale on the right axis). Upper inset shows k_{obs} of the first phase, which is the formation of C(4a)-hydroperoxy-flavin, and lower inset show k_{obs} of the second phase, which is the decay of C(4a)-hydroperoxy-flavin. Open-circle lines are data from the double-mixing experiment, and filled-circle lines are those of the dithionite-reduced enzyme.

Enzyme-Monitored Turnover Experiments. Steady-state kinetics of P2O was investigated using the enzyme-monitored turnover method (*23*, *24*). A solution of P2O (42.4 μM) in 50 mM in sodium phosphate, pH 7.0, at 4 °C (air-saturation) was mixed with various concentrations of glucose in the same buffer (50% oxygen) using the stopped-flow spectrophotometer. After mixing, the oxygen concentration was 0.44 mM, and the enzyme concentration was 21.2 μM. The reactions were monitored at the wavelength 458 nm for measuring the amount of the oxidized enzyme after reaching the steady-state period (~0.5 s) until all oxygen was consumed (Figure 5A). The area under the curves in Figure 5A is therefore proportional to the amount of oxygen left. Initial rates of the reaction at any remaining oxygen concentrations were calculated according to the eqs 3 and 4.

$$v = \frac{dA}{dt}\frac{[O_2]_{total}}{A_{total}} \quad (3)$$

$$[O_2] = [O_2]_{total}\frac{A_{t_1 \rightarrow final}}{A_{total}} \quad (4)$$

where dA = area of each segment that corresponds to a division on the *X*-axis (dt), $dt = t_2 - t_1$ for $t_2 > t_1$, A_{total} = total area under the trace, $A_{t_1}\rightarrow$final = area under the trace from t_1 to the end, and $[O_2]_{total} = 0.44$ mM.

A double-reciprocal plot of initial rates versus oxygen concentrations at various glucose concentrations shows a series of parallel lines (Figure 5B). These results were analyzed according to Dalziel's equation (eq 5) (*25*) and eq 6 as described in ref *26* for a bisubstrate reaction using the Enzfitter program (BIOSOFT, Cambridge, UK) for global analysis; v and V are initial and maximum velocity, respectively. K_a and K_b are the Michaelis constants (K_m) for substrates A and B, respectively. The global analysis indicated the turnover number (k_{cat}) of 8.15 ± 0.15 s^{-1}, K_m^G for D-glucose of 1.90 ± 0.07 mM, and $K_m^{O_2}$ for

Table 2: Apparent Rate Constants of the Oxidative Half-Reaction

reduced P2O prepared by reduction with	k_{app} (M^{-1} s^{-1}) for formation of C4a-hydroperoxy-flavin of the first phase	intercept of the first phase (s^{-1})	k_{app} (s^{-1}) for the decay of the C4a-hydroperoxy-flavin of the second phase
D-glucose	$(4.3 \pm 0.4) \times 10^{4a}$	18^a	21 ± 2^a
	$(4.3 \pm 0.2) \times 10^{4b}$	18^b	24 ± 4^b
dithionite solution	$(4.8 \pm 0.2) \times 10^4$	19	22 ± 2

[a] Apparent rate constants (k_{app}) from single-mixing stopped-flow spectrometry taken from the previous report (*13*)). [b] Apparent rate constants (k_{app}) from double-mixing stopped-flow spectrometry (Figure 4).

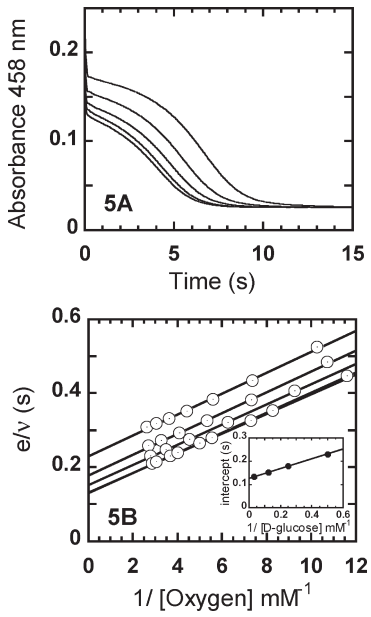

FIGURE 5: Enzyme-monitored turnover experiments. A solution of P2O (42.4 μM) in 50 mM sodium phosphate, pH 7.0, was mixed with D-glucose concentrations of 2, 4, 8, 16, and 32 mM (from right to left traces). Concentrations are as after mixing. (A) The reactions were monitored at 458 mM. (B) A double-reciprocal plot of initial rates versus oxygen concentrations. Lower to upper lines of the primary plot are from the reactions with 32, 16, 8, 4, and 2 mM glucose. In the inset of panel B, the ordinate intercepts from the double-reciprocal plot are plotted as a function of the reciprocal of glucose concentrations.

molecular oxygen of 0.22 ± 0.008 mM (Table 3). The value of k_{cat} (8.15 ± 0.15 s^{-1}) can rule out the involvement of the slow step of 2-keto-D-glucose release (k_4 of 0.002 s^{-1} in Scheme 3) in the catalytic turnover of P2O since this rate is much lower than the k_{cat}. Derivation of the initial rate equation for the model in the upper pathway in Scheme 3 describes the relationship of k_{cat}, K_m^G, $K_m^{O_2}$, and the microscopic rate constants as in eqs 7−10.

$$\frac{e}{v} = \phi_0 + \frac{\phi_G}{[G]} + \frac{\phi_{O_2}}{[O_2]} \quad (5)$$

$$v = \frac{VAB}{K_a B + K_b A + AB} \quad (6)$$

$$\frac{e}{v} = \frac{k_{-2} + k_3}{k_2 k_3} + \frac{1}{k_3} + \frac{1}{k_6} + \frac{(k_{-2} + k_3)}{k_2 k_3 [G]} + \frac{1}{k_5 [O_2]} \quad (7)$$

$$K_m^G = \frac{K_d}{\frac{k_2}{k_{-2}+k_3}\left(1 + \frac{k_3}{k_6}\right) + 1} \quad (8)$$

$$K_m^{O_2} = \frac{1}{k_5\left(\frac{k_{-2}+k_3}{k_2 k_3} + \frac{1}{k_3} + \frac{1}{k_6}\right)} \quad (9)$$

$$k_{cat} = \left[\frac{k_{-2} + k_3}{k_2 k_3} + \frac{1}{k_3} + \frac{1}{k_6}\right]^{-1} \quad (10)$$

k_{cat}, K_m^G, and $K_m^{O_2}$ were calculated from eqs 8−10, and microscopic rate constants obtained from stopped-flow experiments (Table 1) were found to be 7.67 s^{-1}, 3.2 mM, and 0.132 mM (Table 3). This indicates a reasonable agreement between steady-state kinetics parameters obtained from the direct measurement and from calculation according to the model in the upper path of Scheme 3. These data also indicate that the steps of flavin reduction (k_3) and decay of the C4a-hydroperoxy-flavin intermediate (k_6) are main limiting factors in the turnover of P2O.

DISCUSSION

This study reports investigation of the reaction mechanism of pyranose 2-oxidase from *Trametes multicolor* using rapid and steady-state kinetics. The overall kinetic scheme and the individual rate constants associated with each step are described in Scheme 3 and Table 1. Results of steady-state kinetics show a parallel-line pattern instead of an intersecting-line pattern. These data fit with the interpretation that the mechanism of P2O is of the ping-pong-type where the 2-keto-D-glucose product leaves prior to the oxygen reaction (upper path in Scheme 3). Alternatively, the parallel-line pattern also fits with the model that the sugar product remains bound during the reaction with oxygen but the reduction step is essentially irreversible ($k_3 \gg k_{-3}$). Therefore, the binding of oxygen is virtually cut off from the binding of D-glucose, giving a parallel pattern for the double-reciprocal plot (lower path in Scheme 3). In the reaction of D-amino acid oxidase, which occurs through a ternary complex mechanism, the steady-state kinetics shows a parallel-line instead of an intersecting-line pattern because the reverse rate of the flavin reduction step is very small (*27*). This implies that when only steady-state kinetics data alone is considered, the lower pathway of Scheme 3 cannot be ruled out.

However, based on the results of the oxidative half-reaction in the absence and presence of 2-keto-D-glucose, the reaction mechanism of P2O is more likely to be of the ping-pong-type as described in the upper path of Scheme 3. Reoxidation of the reduced enzyme prepared by the reduction with dithioinite ((4.8 ± 0.2) × 10^4 M^{-1} s^{-1}) or D-glucose ((4.3 ± 0.4) × 10^4 M^{-1} s^{-1} (*13*)) yielded similar observed rate constants for formation and decay of C4a-hydroperoxy-FAD. These rate constants are also similar to those from the double-mixing experiment where 2-keto-D-glucose is present ((4.3 ± 0.2) × 10^4 M^{-1} s^{-1}) (Figure 4, Table 2). It is difficult to perceive that kinetics of the oxygen reaction in the absence and presence of 2-keto-D-glucose are the same as shown in Figure 4 if the sugar product remains bound during the oxidative half-reaction as in the lower pathway of Scheme 3. Most of flavoprotein oxidases employing the ternary complex mechanism show effects of product binding on their bimolecular rate constants for flavin oxidation (*16*). In monoamine oxidases (*28*, *29*) and lactate monooxygenase (*30*), the oxidation rates are significantly increased when the products are bound. In dimethylglycine oxidase from *Arthrobacter globiformis*, binding of the product decreases a bimolecular rate constant of the flavin oxidation from 3.42 × 10^5 to 2.01 × 10^5 M^{-1} s^{-1} (*31*). In the case of alditol oxidase from *Streptomyces coelicolor*, the bimolecular rate constant for

Table 3: Steady-State Kinetics Parameters

kinetic parameters	enzyme-monitored turnover	calculation from microscopic rate constants and eq 7
K_m^G	1.9 ± 0.07 mM	3.2 mM
$K_m^{O_2}$	0.22 ± 0.008 mM	0.132 mM
K_{cat}	8.15 ± 0.15 s^{-1}	7.67 s^{-1}

the flavin oxidation is only slightly affected by the presence of the sugar product, 1.7×10^5 M^{-1} s^{-1} for the reaction of the free enzyme versus 1.4×10^5 M^{-1} s^{-1} when D-xylose was used for preparing the reduced enzyme (*32*). However, there is no direct evidence confirming that the oxidized D-xylose was still bound when the reduced enzyme reacted with oxygen during the stopped-flow experiments. In addition, steady-state kinetics of alditol oxidase shows a parallel-line pattern (*32*). In our opinion, it is possible that the oxidized D-xylose product dissociates before the reduced enzyme reacts with oxygen and the reaction of alditol oxidase is a ping-pong-type. In P2O reaction, it is likely that during the double-mixing experiment (Figure 4), although 2-keto-D-glucose was present, it might not remain bound when oxygen diffuses into the active site of the reduced enzyme.

When the kinetic data are considered together with the previous structural knowledge of P2O, the kinetic model as in the upper pathway of Scheme 3 is also favored. The X-ray structure of P2O from *T. multicolor* shows that when it binds to a small molecule such as acetate, the active site of P2O is closed off (closed conformation) from the internal cavity by a dynamic loop, which is similar to the lid structure found in other GMC oxidoreductases (*9*). The loop is in the open conformation when a sugar substrate (2-fluoro-2-deoxy-D-glucose) (*10*) or 2-keto-D-glucose is bound (*11*). The open conformation is proposed to be relevant to the reductive half-reaction since there is more space at the active site to accommodate the sugar binding; in fact the loop in its closed conformation would interfere with the sugar substrate binding (*10*). The closed conformation is compatible with the oxidative half-reaction since the active site is more closed off from the bulk solvent, providing a suitable environment for the formation of a C4a-hydroperoxy-FAD intermediate (*13*, *33*). In this view, the structural data also support the mechanism in the upper pathway of Scheme 3 since the restricted space in the active site of P2O would require the sugar product to leave prior to the formation of C4a-hydroperoxy-FAD. It can be envisaged that during the reductive half-reaction and under anaerobic conditions as in Figure 1, the substrate loop is in the open conformation and the sugar product releases at the rate of 0.002 s^{-1} (k_4 in Scheme 3). The slow releasing of the sugar product in the open conformation may be due to similarity in the structures of D-glucose and 2-keto-D-glucose. In the structure of P2O from *Peniophora* sp, 2-keto-D-glucose is bound at the enzyme in the open conformation (*11*). However, when oxygen is present, the substrate loop moves to attain its closed conformation, causing the active site to be more spatially restricted and unsuited to accommodate simultaneously the formed C4a-hydroperoxy-flavin adduct and 2-keto-D-glucose. Therefore, we propose that the substrate loop movement may be the main feature facilitating the quick release of the sugar product, and it is triggered when oxygen is present during the oxidative half-reaction. It should be mentioned that although a specific binding site for oxygen in flavoenzymes has been a matter of debate, it cannot be completely ruled out since the recent study of cholesterol oxidase shows a hydrophobic tunnel that may serve as a specific binding pathway for oxygen to reach the reduced flavin cofactor (*34*). In P2O case, it may be either the presence of oxygen in the enzyme active site triggering this conformational change or direct diffusion of oxygen to form the C4a-hydroperoxy-flavin adduct intermediate causing the loop movement, resulting in the release of 2-keto-D-glucose.

The proposed ping-pong mechanism in the upper pathway of Scheme 3 was tested for its validity by comparing kinetic constants obtained from pre-steady-state and steady-state kinetics data. The initial rate equation for the upper pathway of Scheme 3 was derived as shown in eq 7. Based on eqs 8−10 and microscopic rate constants obtained from pre-steady-state kinetics, the K_m^G of glucose was calculated to be 3.2 mM whereas the K_m^G measured from the steady-state kinetics is 1.9 ± 0.07 mM (Table 3). The $K_m^{O_2}$ of oxygen calculated from microscopic rate constants and eq 9 is 0.132 mM, whereas the $K_m^{O_2}$ measured from the steady-state kinetics is 0.22 ± 0.008 mM (Table 3). The experimental and calculated values of K_m^G and $K_m^{O_2}$ are in the same range, indicating that the ping-pong model as in the upper path of Scheme 3 is valid for the reaction mechanism of P2O. In addition, simulations of the kinetic mechanism of Scheme 2 yielded kinetic traces that agree well with the experimental data (Figure 1A) and simulations of the oxidative half-reaction reported previously also show good agreement with the experimental data (*13*).

Pre-steady-state kinetics studies on the reductive half-reaction of P2O using 2-*d*-D-glucose showed interesting results that gave additional insight into the reaction mechanism of P2O. The reaction with the deuterated substrate (2-*d*-D-glucose) shows a large primary kinetic isotope effect ($k_{3H}/k_{3D} = 8.84$) on the FAD reduction (Figure 3), confirming that P2O oxidizes D-glucose at position C2 as previously reported (*1*). It also indicates that the C−H moiety at the C2 position is the reducing equivalent used for FAD reduction and that breakage of this C−H bond occurs simultaneously with FAD reduction. The reaction mechanism of P2O possibly occurs by the hydride transfer mechanism generally proposed for the enzymatic oxidation of alcohols (*35*). Activation for alcohol substrates has been proposed to be initiated by the removal of the hydroxyl proton from the alcohols, followed by the transfer of the hydride moiety (*35*−*37*). This mechanism proceed stepwise by initially forming an alkoxide species that is decoupled from the following C−H bond cleavage as found in the reaction of choline oxidase (*38*) or concerted. In the GMC oxidoreductase family, histidine residues are generally found to be conserved and were proposed as a general catalytic base in the deprotonation of the substrate hydroxyl group in order to promote the hydride transfer (*35*, *39*). His516 is probably the base abstracting the hydroxyl proton in the reaction of glucose oxidase (*40*), and homologous histidines in methanol oxidase (*39*) and cellobiose dehydrogenase (*41*) are proposed to fulfill the

same function. In P2O, the residues His548 and Asn593 are conserved as found in most members of the GMC family except glucose oxidase in which only the histidine−histidine pair was found instead (*9*). The three-dimensional structure of P2O modeled with the substrate D-glucose has shown that the distance from the C2 site of D-glucose to the N(5) of the flavin ring is 3.1 Å, suggesting that the hydride transfer mechanism is possible (*10*). In addition, the residues His548 and Asn593 can participate in hydrogen bonding of the C2−OH of the sugar (*10*), indicating that His548 may act as a reactive base in proton abstraction. However, the direct role of the histidine residue in the hydroxyl proton abstraction in the GMC family has never been clearly demonstrated. The high-resolution X-ray structure of cholesterol oxidase (type I) from *Streptomyces* sp. shows that the conserved histidine residue (His447) is protonated and therefore cannot act as a catalytic base (*42*). The pH−rate profiles of His466Ala and His351Ala of choline oxidase are similar to that of the wild-type enzyme. This indicates that a base that is required to be in the deprotonated state still remains in these mutants, implying that neither His466 nor His351 alone act as the active-site base (*43*, *44*). These histidine residues in both cholesterol and choline oxidases may help in providing the suitable environment for catalysis (*42*) or hydride tunneling (*45*).

The detection of the formation of the enzyme−substrate complex as evident by the increase of absorbance at 395 during the first phase of the reductive half-reaction of P2O (Figure 1A) and the inverse isotope effect associated with this step (Figure 2A and 3, Table 1) are quite intriguing and provide useful information about the nature of the substrate binding. The spectroscopic change upon substrate binding has not been shown for other enzymes in the GMC oxidoreductase family such as methanol oxidase (*46*), glucose oxidase (*47*, *48*), cholesterol oxidase (*49*, *50*), and choline oxidase (*38*, *51*). This absorbance change cannot be flavin semiquinone formation or N(5) or C(4a) flavin adduct formation since there is no absorbance change at 458 nm. Although a similar absorbance increase at 400 nm was documented for the ionization of the imidazole moiety of 8α-histidylriboflavin, which displays a pK_a of 4.7 (*52*), it is unlikely that in the case of P2O, the intermediate spectrum is caused by the same ionization. Absorption spectra of P2O in the pH range of 5.5−9 are the same and indicate no change in this area (data not shown). It is possible that this absorbance change is due a close contact between D-glucose and the oxidized FAD. However, based on current data, the structural nature of this intermediate cannot be identified and requires future investigation (see paragraph below) before any conclusion can be drawn.

The binding of D-glucose or 2-*d*-D-glucose to the enzyme is a two-step process (Schemes 2 and 3). The initial complex formation in the first step (Scheme 2) shows an insignificant isotope effect on the initial binding since the K_d values are in the same range, ~45 mM for D-glucose versus ~60 mM for 2-*d*-D-glucose (Figure 2B). This indicates that the C2−H bonds in the free D-glucose and in the D-glucose of the initial complex are similar. Interestingly, the following isomerization step (k_2 in Schemes 2 and 3) shows an inverse isotope effect (k_{2H}/k_{2D} of ~0.60). This indicates that upon isomerization to the active P2O−glucose complex, the C2−H bond is stiffer and more constrained compared with that in the free D-glucose (*53*, *54*). However, since the accuracy of k_{2H}/k_{2D} measured experimentally is limited due to limitation of the measurement, at this point, we refrain from making any mechanistic interpretation of the inverse isotope effect observed.

In conclusion, this study has elucidated the kinetic mechanism of pyranose 2-oxidase from *Trametes multicolor*. Our results suggest that at pH 7.0, the P2O reaction is likely to be the ping-pong type where the sugar product leaves prior to the oxygen reaction. Binding of the oxidized enzyme to D-glucose shows an absorbance increase at 395 nm and an inverse isotope effect, indicating that the C2−H bond of D-glucose is more rigid in the Michaelis complex compared with that in the free form. This information can serve as the grounds for future in-depth investigation into the reaction and mechanism of P2O.

REFERENCES

1. Leitner, C., Volc, J., and Haltrich, D. (2001) Purification and characterization of pyranose oxidase from the white rot fungus *Trametes multicolor*. *Appl. Environ. Microbiol. 67*, 3636–3644.
2. Giffhorn, F. (2000) Fungal pyranose oxidases: Occurrence, properties and biotechnical applications in carbohydrate chemistry. *Appl. Microbiol. Biotechnol. 54*, 727–740.
3. Shah, V., and Nerud, F. (2002) Lignin degrading system of white-rot fungi and its exploitation for dye decolorization. *Can. J. Microbiol. 48*, 857–870.
4. van Hellemond, E. W., Leferink, N. G. H., Heuts, D. P. H. M., Fraaije, M. W., and van Berkel, W. J. H. (2006) Occurrence and biocatalytic potential of carbohydrate oxidase. *Adv. Appl. Microbiol. 60*, 17–54.
5. Haltrich, D., Leitner, C., Neuhauser, W., Nidetzky, B., Kulbe, K. D., and Volc, J. (1998) A convenient enzymatic procedure for the production of aldose-free-D-tagatose. *Ann. N.Y. Acad. Sci. 864*, 295–299.
6. Volc, J., Kubátová, E., Sedmera, P., Daniel, G., and Gabriel, J. (1991) Pyranose oxidase and pyranosone dehydratase: Enzymes responsible for conversion of D-glucose to cortalcerone by the basidiomycete *Phanerochaete chrysosporium*. *Arch. Microbiol. 156*, 297–301.
7. Halada, P., Leitner, C., Sedmera, P., Haltrich, D., and Volc, J. (2003) Identification of the covalent flavin adenine dinucleotide-binding region in pyranose 2-oxidase from *Trametes multicolor*. *Anal. Biochem. 314*, 235–242.
8. Albrecht, M., and Lengauer, T. (2003) Pyranose oxidase identified as a member of the GMC oxidoreductase family. *Bioinformatics 19*, 1216–1220.
9. Hallberg, B. M., Leitner, C., Haltrich, D., and Divne, C. (2004) Crystal structure of the 270 kDa homotetrameric lignin-degrading enzyme pyranose 2-oxidase. *J. Mol. Biol. 341*, 781–796.
10. Kujawa, M., Ebner, H., Leitner, C., Hallberg, B. M., Prongjit, M., Sucharitakul, J., Ludwig, R., Rudsander, U., Peterbauer, C., Chaiyen, P., Haltrich, D., and Divne, C. (2006) Structural basis for substrate binding and regioselective oxidation of monosaccharides at C3 by pyranose 2-oxidase. *J. Biol. Chem. 281*, 35104–35115.
11. Bannwarth, M., Heckmann-Pohl, D., Bastian, S., Giffhorn, F., and Schulz, G. E. (2006) Reaction geometry and thermostable variant of pyranose 2-oxidase from the white-rot fungus *Peniophora* sp. *Biochemistry 45*, 6587–6595.
12. Rungsrisuriyachai, K., and Gadda, G. (2009) A pH switch affects the steady-state kinetic mechanism of pyranose 2-oxidase from *Trametes ochracea*. *Arch. Biochem. Biophys. 483*, 10–15.
13. Sucharitakul, J., Prongjit, M., Haltrich, D., and Chaiyen, P. (2008) Detection of a C4a-hydroperoxyflavin intermediate in the reaction of a flavoprotein oxidase. *Biochemistry 47*, 8485–8490.
14. Orville, A. M., Lountos, G. T., Finnegan, S., Gadda, G., and Prabhaka, R. (2009) Crytallographic, spectroscopic, and computational analysis of flavin C4a-oxygen adduct in choline oxidase. *Biochemistry 48*, 720–728.
15. Palfey, B. A., and Massey, V. (1998) Flavin-dependent enzymes, in *Comprehensive Biological Catalysis* (Michael, S., Ed.) Vol. *3*, pp 83−153, Academic Press, San Diego, CA.
16. Mattevi, A. (2006) To be or not to be an oxidase: Challenging the oxygen reactivity of flavoenzymes. *Trends Biochem. Sci. 31*, 276–283.

17. Danneel, H. J., Rossner, E., Zeeck, A., and Giffhorn, F. (1993) Purification and characterization of a pyranose oxidase from the basidiomycete *Peniophora gigantea* and chemical analyses of its reaction products. *Eur. J. Biochem. 214*, 795–802.
18. Sucharitakul, J., Phongsak, T., Entsch, B., Svasti, J., Chaiyen, P., and Ballou, D. P. (2007) Kinetics of a two-component *p*-hydroxyphenylacetate hydroxylase explain how reduced flavin is transferred from the reductase to the oxygenase. *Biochemistry 46*, 8611–8623.
19. Hammes, G. G., and Schimmel, R. P. (1966) Chemical relaxation spectra: Calculation of relaxation times for complex mechanisms. *J. Phys. Chem. 70*, 2319–2324.
20. Hammes, G. G., and Schimmel, R. P. (1967) Relaxation spectra of enzymic reactions. *J. Phys. Chem. 71*, 917–923.
21. Hiromi, K. (1979) Analysis of fast enzyme reactions: Transient kinetics, *Kinetics of Fast Enzyme Reactions: Theory and Practice*, pp 187−244, Kodansha Ltd., Tokyo.
22. Fisher, F. H. (2005) Transient-state kinetic approach to mechanisms of enzyme catalysis. *Acc. Chem. Res. 38*(3), 157–166.
23. Chance, B. (1943) The kinetics of the enzyme-substrate compound of peroxidase. *J. Biol. Chem. 151*, 553–557.
24. Gibson, H. Q., Swoboda, E. P. B., and Massey, V. (1964) Kinetics and mechanism of action of glucose oxidase. *J. Biol. Chem. 239*, 3927–3933.
25. Dalziel, K. (1957) Initial steady state velocities in the evauation of enzyme-coenzyme- substrate reaction mechanisms. *Acta Chem. Scand. 11*, 1706–1723.
26. Cook, P. E., and Cleland, W. W. (2007) Initial velocity studies in the absence of added inhibiter, in *Enzyme Kinetics and Mechanism* (Rogers, R. L., and Scholl, S., Eds.) pp 59−204, Garland Science Publishing, New York.
27. Fitzpatrick, P. F., and Massey, V. (1982) The kinetic mechanism of D-amino acid oxidase with D-alpha-aminobutyrate as substrate. Effect of enzyme concentration on the kinetics. *J. Biol. Chem. 257*, 12916–12923.
28. Tan, A. K., and Ramsay, R. R. (1993) Substrate-specific enhancement of the oxidative half-reaction of monoamine oxidase. *Biochemistry 32*, 2137–2143.
29. Edmonson, D. E., Binda, C., and Mattevi, A. (2007) Structural insights into the mechanism of amine oxidation by monoamine oxidases A and B. *Arch. Biochem. Biophys. 464*, 269–276.
30. Sun, W., Williams, C. H.Jr., and Massey, V. (1997) The role of glycine 99 in L-lactate monooxygenase from *Mycobacterium smegmatis*. *J. Biol. Chem. 272*, 27065–27076.
31. Basran, J., Bhanji, N., Basran, A., Nietlispach, D., Mistry, S., Meskys, R., and Scrutton, N. S. (2002) Mechanistic aspects of the covalent flavoprotein dimethylglycine oxidase of *Arthrobacter globiformis* studied by stopped-flow spectrophotometry. *Biochemistry 41*, 4733–4743.
32. Heuts, D. P, van Hellemond, E. W, Janssen, D. B, and Fraaije, M. W. (2007) Discovery, characterization, and kinetic analysis of an alditol oxidase from *Streptomyces coelicolor*. *J. Biol. Chem. 282*, 20283–20291.
33. Alfieri, A., Fersini, F., Ruangchan, N., Prongjit, M., Chaiyen, P., and Mattevi, A. (2007) Structure of the monooxygenase component of a two-component flavoprotein monooxygenase. *Proc. Natl. Acad. Sci. U.S.A. 104*, 1177–1182.
34. Chen, L., Lyubimov, A. Y., Brammer, L., Vrielink, A., and Sampson, N. S. (2008) The binding and release of oxygen and hydrogen peroxide are directed by a hydrophobic tunnel in cholesterol oxidase. *Biochemistry 47*, 5368–5377.
35. Fitzpatrick, P. F. (2001) Substrate dehydrogenation by flavoproteins. *Acc. Chem. Res. 34*, 299–307.
36. Cook, P. F., and Cleland, W. W. (1981) pH variation of isotope effects in enzyme-catalyzed reactions. 2. Isotope-dependent step not pH dependent. Kinetic mechanism of alcohol dehydrogenase. *Biochemistry 20*, 1805–1816.
37. Sekhar, V. C., and Plapp, B. V. (1990) Rate constants for a mechanism including intermediates in the interconversion of ternary complexes by horse liver alcohol dehydrogenase. *Biochemistry 29*, 4289–4295.
38. Fan, F., and Gadda, G. (2005) On the catalytic mechanism of choline oxidase. *J. Am. Chem. Soc. 127*, 2067–2074.
39. Menon, V., Hsieh, C-T., and Fitzpatrick, P. E. (1995) Substituted alcohols as mechanistic probes of alcohol oxidase. *Bioorg. Chem. 23*, 42–53.
40. Wohlfahrt, G., Trivić, S., Zeremski, J., Pericin, D., and Leskovac, V. (2004) The chemical mechanism of action of glucose oxidase from Aspergillus niger. *Mol. Cell. Biochem. 260*, 69–83.
41. Rotsaert, F. A., Hallberg, B. M., de Vries, S., Moenne-Loccoz, P., Divne, C., Renganathan, V., and Gold, M. H. (2003) Biophysical and structural analysis of a novel heme B iron ligation in the flavocytochrome cellobiose dehydrogenase. *J. Biol. Chem. 278*, 33224–33231.
42. Sampson, N. S., and Vrielink, A. (2003) Cholesterol oxidases: A study of Nature's approach to protein design. *Acc. Chem. Res. 36*, 713–722.
43. Ghanem, M., and Gadda, G. (2005) On the catalytic role of the conserved active site residue His466 of choline oxidase. *Biochemistry 44*, 893–904.
44. Rungsrisuriyachai, K., and Gadda, G. (2008) On the role of histidine 351 in the reaction of alcohol oxidation catalyzed by choline oxidase. *Biochemistry 47*, 6762–6769.
45. Fan, F., and Gadda, G. (2007) An internal equilibrium preorganizes the enzyme−substrate complex for hydride tunneling in choline oxidase. *Biochemistry 46*, 6402–6408.
46. Sherry, B., and Abeles, R. H. (1985) Mechanism of action of methanol oxidase, reconstitution of methanol oxidase with 5-deazaflavin, and inactivation of methanol oxidase by cyclopropanol. *Biochemistry 24*, 2594–2605.
47. Gibson, Q. H., Swoboda, B. E., and Massey, V. (1964) Kinetics and mechanism of glucose oxidase. *J. Biol. Chem. 239*, 3927–3934.
48. Weibel, M. K., and Bright, H. J. (1971) The glucose oxidase mechanism. Interpretation of the pH dependence. *J. Biol. Chem. 246*, 2734–2744.
49. Pollegioni, L., Wels, G., Pilone, M. S., and Ghisla, S. (1999) Kinetic mechanisms of cholesterol oxidase from *Streptomyces hygroscopicus* and *Brevibacterium sterolicum*. *Eur. J. Biochem. 264*, 140–151.
50. Lim, L., Molla, G., Guinn, N., Ghisla, S., Pollegioni, L., and Vrielink, A. (2006) Structural and kinetic analyses of the H121A mutant of cholesterol oxidase. *Biochem. J. 400*, 13–22.
51. Fan, F., Germann, M. W., and Gadda, G. (2006) Mechanistic studies of choline oxidase with betaine aldehyde and its isosteric analogue 3,3-dimethylbutyraldehyde. *Biochemistry 45*, 1979–1986.
52. Walker, W. H., Singer, T. P., Ghisla, S., and Hemmerich, P. (1972) Studies on succinate dehydrogenase. 8α-Histidyl-FAD as the active center of succinate dehydrogenase. *Eur. J. Biochem. 26*, 279–289.
53. Schramm, V. L. (2007) Binding isotope effects: Boon and bane. *Curr. Opin. Chem. Biol. 11*, 529–536.
54. Cook, P. E., and Cleland, W. W. (2007) Isotope Effects as a Probe of Mechanism, in *Enzyme Kinetics and Mechanism* (Rogers, R. L., and Scholl, S., Eds.) pp 253−321, Garland Science Publishing, New York.